Progress In Electromagnetics Research, Vol. 125, 365–389, 2012

THE THRESHOLD MODE STRUCTURE ANALYSIS OF THE TWO-DIMENSIONAL PHOTONIC CRYSTAL LASERS

M. Koba[1, 2, 3, *] and P. Szczepanski[2, 3]

[1]Institute of Experimental Physics, University of Warsaw, 69 Hoza St., Warsaw 00-681, Poland

[2]Institute of Microelectronics and Optoelectronics, Warsaw University of Technology, 75 Koszykowa St., Warsaw 00-662, Poland

[3]National Institute of Telecommunications, 1 Szachowa St., Warsaw 04-894, Poland

Abstract—In this work, threshold mode structures of two-dimensional (2D) photonic crystal (PC) lasers are presented. The subjects of this paper are finite photonic crystal structures with circular holes arranged in square and triangular lattices. In each case, both transverse magnetic (TM) and transverse electric (TE) polarization are studied. The analysis is based on the coupled-wave equations and analyzes modes' behavior for the wide range of coupling coefficient values. The laser mode is characterized by threshold gain and frequency deviation, and these quantities depend on coupling constants, which means that the threshold gain of the mode and the mode's frequency deviation depend on the coupling constants. Presented analysis gives an interesting insight into behavior of the modes in photonic crystal lasers.

1. INTRODUCTION

Recently, there has been increasing interest in two-dimensional (2D) photonic crystal (PC) lasers utilizing a 2D distributed feedback (DFB) mechanism. They have been attracting much attention because of their important characteristics, such as single mode operation in a large cavity area and a diffraction-limited circular-shape output beam [1, 2]. The PC laser demonstrations were obtained under pulse excitation,

Received 12 January 2012, Accepted 17 February 2012, Scheduled 5 March 2012

* Corresponding author: Marcin Koba (mkoba@elka.pw.edu.pl).

weather optical or electrical, as well as continues wave regime [3–11]. Simultaneously, theoretical models of PC laser structures have been developed [12–19]. Particularly, coupled-wave models for square and triangular lattices 2D PC lasers with transverse electric and transverse magnetic like modes have been presented. In [16, 17], the coupled-wave equations and field distributions for square lattice PC laser were shown for TE and TM modes, respectively.

In [15], the expressions for the resonant frequencies of mode derived from the coupled-mode equations describing the characteristics of experimental results for the band-edge frequencies of the 2D PC laser are shown. In the case of TM-like modes [17], the threshold characteristics for this kind of laser structures have been obtained. It is also shown that this lasing mode can be selected by manipulating the filling factor or the boundary reflection. In order to further develop the PC laser, it seems to be important to investigate different crystal geometries such as triangular lattice. A PC laser with triangular lattice geometry has been studied [3, 4] and was found to have six resonant modes at the edge of photonic band structure. Some of the resonant properties have been studied in further works [7, 12]. Recently, coupled-wave model for triangular-lattice photonic crystal with transverse electric polarization has been presented [18]. The analytic expressions that describe the relations between the resonant mode frequencies and coupling constant have been derived. However, it is also important to understand the resonant modes with TM polarization, since for example the promising light sources for TM region (e.g., quantum cascade lasers) have their gain in TM polarization [20]. In this paper, two cases of photonic crystal symmetries (square and triangular) and TE and TM polarizations, for each structure, are analyzed. In comparison with earlier works, this one gathers all four possible scenarios and analyzes them in the wide range of the coupling coefficient values, extending the two-dimensional coupled-wave model for triangular lattice photonic crystal laser to describe threshold behavior of the TM-like modes.

2. COUPLED-WAVE MODELS

Throughout this work a PC structure in a fixed square area with circular holes arranged in square or triangular lattice is considered. Following works of, e.g., Plihal and Maradudin [14] and Sakai et al. [2, 16–18], four cases are distinguished: PC cavity with square and triangular lattices with, in each case, TE and TM modes. The discussed structures are schematically shown in Figure 1. These structures are assumed to be uniform and not confined in the z

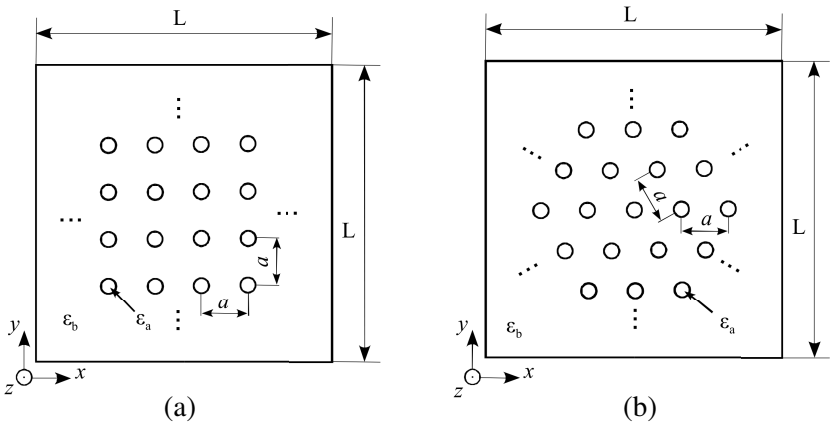

Figure 1. A schematic cross section of (a) square and (b) triangular lattice photonic crystal structures.

direction.

The scalar wave equations for the electric and magnetic fields, E_z and H_z, respectively, are written in the following form [14]:

$$\frac{\partial^2 E_z}{\partial x^2} + \frac{\partial^2 E_z}{\partial y^2} + k^2 E_z = 0 \tag{1}$$

and

$$\frac{\partial}{\partial x}\left\{\frac{1}{k^2}\frac{\partial}{\partial x}H_z\right\} + \frac{\partial}{\partial y}\left\{\frac{1}{k^2}\frac{\partial}{\partial y}H_z\right\} + H_z = 0 \tag{2}$$

In Equations (1) and (2), the constant k is given by:

$$k^2 = \beta^2 + 2i(\alpha - \alpha_L)\beta + 2\beta \sum_{\mathbf{G}\neq 0} \kappa(\mathbf{G}) \exp\left(i\left(\mathbf{G}\cdot\mathbf{r}\right)\right) \tag{3}$$

in case of TM mode [17] and by

$$\frac{1}{k^2} = \frac{1}{\beta^4}\left(\beta^2 - i2(\alpha - \alpha_L)\beta + 2\beta \sum_{\mathbf{G}\neq 0} \kappa(\mathbf{G}) \exp\left(i\left(\mathbf{G}\cdot\mathbf{r}\right)\right)\right) \tag{4}$$

in case of TE mode [18]. In Equations (3) and (4) $\beta = 2\pi\varepsilon_0^{1/2}/\lambda$ where $\varepsilon_0 = \varepsilon(\mathbf{G} = 0)$ is the averaged dielectric permittivity ($\varepsilon_0^{1/2}$ corresponds to averaged refractive index n), α an averaged gain in the medium, $\kappa(\mathbf{G})$ the coupling constant, λ the Bragg wavelength, $\mathbf{G} = (m\mathbf{b}_1, n\mathbf{b}_2)$ the reciprocal lattice vector, and m and n the arbitrary integers. $\mathbf{b}_1$ and $\mathbf{b}_2$ vary depending on the structure symmetry. Therefore, these vectors are expressed in the following forms $\mathbf{b}_1 = (\beta_0^s, 0)$ and

$\mathbf{b}_2 = (0, \beta_0^s)$ for square lattice, and $\mathbf{b}_1 = (\beta_0^t, 0)$ and $\mathbf{b}_2 = (-\frac{\beta_0^t}{2}, \frac{\sqrt{3}\beta_0^t}{2})$ for triangular lattice structure, where $\beta_0^s = 2\pi/a$ and $\beta_0^t = 4\pi/\sqrt{3}a$. In the derivation of Equations (3) and (4) following e.g., [17, 21], we set $\alpha \ll \beta \equiv \frac{2\pi\varepsilon_0^{1/2}}{\lambda}$, $\varepsilon_{\mathbf{G}\neq 0} \ll \varepsilon_0$, and $\alpha_{\mathbf{G}} \ll \beta$. In these equations, the periodic variation in the refractive index is included as a small perturbation and appears in the third term through the coupling constant $\kappa(\mathbf{G})$ of the form:

$$\kappa(\mathbf{G}) = -\frac{\pi}{\lambda\varepsilon_0^{1/2}}\varepsilon(\mathbf{G}) \pm i\frac{\alpha(\mathbf{G})}{2} \tag{5}$$

In (5), plus sign refers to TM polarization (3), while minus sign refers to TE polarization (4). Further, we set $\alpha(\mathbf{G})|_{\mathbf{G}\neq 0} = 0$ neglecting spatial periodicity of gain. In the vicinity of the Bragg wavelength, some of the diffraction orders contribute to the coupling of waves in more significant way than the others. In general, a periodic perturbation produces an infinite set of diffraction orders. The Bragg frequency corresponding to the Γ point in the photonic band structure [12] is chosen for the purpose of this paper, and the most significantly contributing coupling constants are expressed as follows:

$$\kappa_1 = \kappa(\mathbf{G})\big|_{|\mathbf{G}|=\beta_0^{s,t}} \quad \kappa_2 = \kappa(\mathbf{G})\big|_{|\mathbf{G}|=\sqrt{3}\beta_0^{s,t}} \quad \kappa_3 = \kappa(\mathbf{G})\big|_{|\mathbf{G}|=2\beta_0^{s,t}} \tag{6}$$

In Equations (1) and (2), electric and magnetic fields for the infinite periodic structure are given by the Bloch mode [14]:

$$E_z(\mathbf{r}) = \sum_{\mathbf{G}} e(\mathbf{G}) \exp\left(i\left(\mathbf{k}+\mathbf{G}\right)\cdot\mathbf{r}\right) \tag{7}$$

and

$$H_z(\mathbf{r}) = \sum_{\mathbf{G}} h(\mathbf{G}) \exp\left(i\left(\mathbf{k}+\mathbf{G}\right)\cdot\mathbf{r}\right) \tag{8}$$

where functions $e(\mathbf{G})$ and $h(\mathbf{G})$ correspond to the plane wave amplitudes, whereas wave vector is denoted by $\mathbf{k}$. It is worth noting here that for the more general three-dimensional case with vertical confinement (i.e., in z direction) only the waves diffracted in the plane should be included, e.g., [24]. In the first Brillouin zone $\mathbf{k} = 0$ at the Γ point [16–18]. For a finite structure, the amplitude of each plane wave is not a constant, so $e(\mathbf{G})$ and $h(\mathbf{G})$ become functions of space. At the Γ point, we consider only the amplitudes ($e(\mathbf{G})$, $h(\mathbf{G})$) which are the most significant and let include one- and two-dimensional coupling effects, i.e., in most cases with $|\mathbf{G}| = \beta_0^{s,t}$, except for square lattice with TE polarization where additional $h(\mathbf{G})$ amplitudes with $|\mathbf{G}| = \sqrt{2}\beta_0^s$ have to be included [15]. For the purpose of this article, the

contributions of higher order waves in the Bloch mode are considered negligible, which in general is not true, especially for non circular holes, e.g., [24, 25].

2.1. Square Lattice

2.1.1. TM Polarization

Considering square lattice photonic crystal with TM polarization, it is assumed that at the Γ point, the most significant contribution to coupling is given by the electric waves, which fulfill the condition ($|\mathbf{G}| = \beta_0^s$). Thus, all higher order electric wave expansion coefficients ($|\mathbf{G}| \geq \sqrt{2}\beta_0$) are neglected. Four basic waves most significantly contributing to coupling are depicted in Figure 2.

Equation (7) describes infinite structures. It is possible to take into account the fact that the structure is finite by using the space dependent amplitudes, e.g., [15]. Thus, the electric field (7) in the finite periodic structure can be expressed in the following way:

$$E_z = E_1^s(x,y)e^{-i\beta_0^s x} + E_2^s(x,y)e^{i\beta_0^s x} + E_3^s(x,y)e^{-i\beta_0^s y} + E_4^s(x,y)e^{i\beta_0^s y} \quad (9)$$

In (9) E_i^s, $i = 1 \ldots 4$ are the four basic electric field amplitudes of waves propagating in four directions $+x$, $-x$, $+y$, y. These amplitudes correspond to $e(\mathbf{G})$ in Equation (7). In further analysis, the space dependence notation is omitted.

Putting Equations (3) and (9) into Equation (1), and assuming the slow varying electromagnetic field, one can get the set of coupled mode equations [17]:

$$-\frac{\partial}{\partial x}E_1^s + (\alpha - \alpha_L - \kappa_0 - i\delta)\, E_1^s = (i\kappa_3 - \kappa_0)\, E_3^s + i\kappa_2\, (E_2^s + E_4^s) \quad (10)$$

$$\frac{\partial}{\partial x}E_3^s + (\alpha - \alpha_L - \kappa_0 - i\delta)\, E_3^s = (i\kappa_3 - \kappa_0)\, E_1^s + i\kappa_2\, (E_2^s + E_4^s) \quad (11)$$

$$-\frac{\partial}{\partial y}E_2^s + (\alpha - \alpha_L - \kappa_0 - i\delta)\, E_2^s = (i\kappa_3 - \kappa_0)\, E_4^s + i\kappa_2\, (E_1^s + E_3^s) \quad (12)$$

$$\frac{\partial}{\partial y}E_4^s + (\alpha - \alpha_L - \kappa_0 - i\delta)\, E_4^s = (i\kappa_3 - \kappa_0)\, E_2^s + i\kappa_2\, (E_1^s + E_3^s) \quad (13)$$

where

$$\delta = (\beta^2 - \beta_0^{s2})/2\beta \approx \beta - \beta_0^s \quad (14)$$

is the Bragg frequency deviation, κ_2 and κ_3 are coupling coefficients [18]. The κ_2 coefficient is responsible for orthogonal coupling (e.g., the coupling of E_1^s to E_2^s and E_4^s), and κ_2 corresponds to backward coupling (e.g., the coupling of E_1^s to E_3^s). The additional coef-

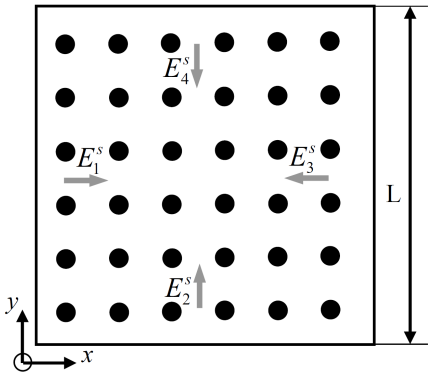

Figure 2. Schematic cross section of square lattice photonic crystal laser active region, where the four basic waves involved in coupling for TM polarization are shown.

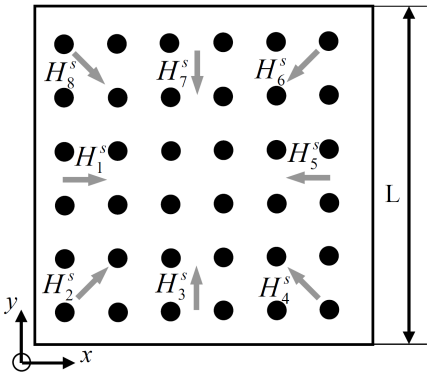

Figure 3. Schematic cross section of square lattice photonic crystal laser active region, where the eight basic waves involved in coupling for TE polarization are shown.

ficient κ_0 denotes surface emission losses [16, 17]. Solution of Equations (10)–(13) for the boundary conditions:

$$E_1^s\left(-\frac{L}{2},y\right)=E_3^s\left(\frac{L}{2},y\right)=0,\quad E_2^s\left(x,-\frac{L}{2}\right)=E_4^s\left(x,\frac{L}{2}\right)=0 \quad (15)$$

defines eigenmodes of the photonic structure. The analysis of this solution will be shown in Section 3.

2.1.2. TE Polarization

In the square lattice photonic crystal cavity with TE polarization, as mentioned before, the coupling process involves magnetic waves satisfying following conditions ($|\mathbf{G}| = \beta_0$) and ($|\mathbf{G}| = \sqrt{2}\beta_0$) [16], neglecting higher order Bloch modes. Eight basic waves most significantly contributing to coupling are depicted in Figure 3.

Similar as in the case of TM polarization, the equation for magnetic field (8) describes modes for infinite structure. Thus, the finite dimensions of the structure are described by spatial dependence of magnetic field amplitudes [16], and the magnetic field (8) is written in the following form:

$$\begin{aligned} H_z(\mathbf{r}) \;=\; & H_1^s(x,y)e^{-i\beta_0^s x}+H_5^s(x,y)e^{i\beta_0^s x}+H_3^s(x,y)e^{-i\beta_0^s y} \\ & +H_7^s(x,y)e^{i\beta_0^s y}+H_2^s(x,y)e^{-i\beta_0^s x-i\beta_0^s y}+H_4^s(x,y)e^{i\beta_0^s x-i\beta_0^s y} \\ & +H_6^s(x,y)e^{i\beta_0^s x+i\beta_0^s y}+H_8^s(x,y)e^{-i\beta_0^s x+i\beta_0^s y} \end{aligned} \quad (16)$$

In Equation (16), H_i^s, $i = 1 \ldots 8$ are the eight basic magnetic field amplitudes of waves propagating in directions schematically shown in Figure 3. These amplitudes correspond to $h(\mathbf{G})$ in Equation (8). Joining Equations (4), (16), and (2), and assuming slowly varying amplitudes, the coupled-wave equations for TE modes in square lattice PC are obtained:

$$\begin{aligned} & -\frac{\partial}{\partial x}H_1^s + (\alpha - \alpha_L - \kappa_0 - i\delta)H_1^s \\ = \; & (i\kappa_3 - \kappa_0)H_5^s + i\frac{2\kappa_1^2}{\beta_0^s}(2H_1^s + H_3^s + H_7^s) \end{aligned} \tag{17}$$

$$\begin{aligned} & \frac{\partial}{\partial x}H_5^s + (\alpha - \alpha_L - \kappa_0 - i\delta)H_5^s \\ = \; & (i\kappa_3 - \kappa_0)H_1^s + i\frac{2\kappa_1^2}{\beta_0^s}(2H_5^s + H_3^s + H_7^s) \end{aligned} \tag{18}$$

$$\begin{aligned} & -\frac{\partial}{\partial x}H_3^s + (\alpha - \alpha_L - \kappa_0 - i\delta)H_3^s \\ = \; & (i\kappa_3 - \kappa_0)H_7^s + i\frac{2\kappa_1^2}{\beta_0^s}(2H_3^s + H_1^s + H_5^s) \end{aligned} \tag{19}$$

$$\begin{aligned} & \frac{\partial}{\partial x}H_7^s + (\alpha - \alpha_L - \kappa_0 - i\delta)H_7^s \\ = \; & (i\kappa_3 - \kappa_0)H_3^s + i\frac{2\kappa_1^2}{\beta_0^s}(2H_7^s + H_1^s + H_5^s) \end{aligned} \tag{20}$$

In the derivation of the above equations, the derivatives of slowly varying amplitudes H_i^s, $i = 2$, 4, 6, 8 and terms much smaller than δ were neglected. In Equations (17)–(20), δ is the Bragg frequency deviation, given by (14). The expressions for the coupling coefficients κ_1, κ_2, and κ_3 can be found in [16, 18].

In contrast to TM polarization, in Equations (17)–(20), the coupling coefficient κ_2 responsible for coupling in perpendicular direction vanishes. The coupling coefficient κ_3 has the same meaning as described in the previous case, whereas the coupling coefficient κ_1 describes, for example, the coupling of waves H_1^s, H_2^s, and H_8^s.

Solution of Equations (17)–(20) while taking into account boundary conditions:

$$H_7^s\left(-\frac{L}{2}, y\right) = H_5^s\left(\frac{L}{2}, y\right) = 0, \quad H_3^s\left(x, -\frac{L}{2}\right) = H_7^s\left(x, \frac{L}{2}\right) = 0 \tag{21}$$

defines structure eigenmodes at lasing threshold, i.e., in the linear case.

2.2. Triangular Lattice

2.2.1. TM Polarization

In the triangular lattice photonic crystal cavity with TM polarization, the coupling process involves waves satisfying following conditions ($|\mathbf{G}| = \beta_0$) [18, 19], neglecting higher order Bloch modes. Six basic waves most significantly contributing to coupling are depicted in Figure 4.

The space dependent amplitudes for electric field $e(\mathbf{G})$ (Equation (7)) in triangular lattice photonic crystal cavity are written in the following form [19]:

$$E_z = E_1^t(x,y)e^{-i\beta_0^t x} + E_2^t(x,y)e^{-i\frac{\beta_0^t}{2}x - i\frac{\sqrt{3}\beta_0^t}{2}y} + E_3^t(x,y)e^{i\frac{\beta_0^t}{2}x - i\frac{\sqrt{3}\beta_0^t}{2}y} + E_4^t(x,y)e^{i\beta_0^t x} + E_5^t(x,y)e^{i\frac{\beta_0^t}{2}x + i\frac{\sqrt{3}\beta_0^t}{2}y} + E_6^t(x,y)e^{-i\frac{\beta_0^t}{2}x + i\frac{\sqrt{3}\beta_0^t}{2}y} \quad (22)$$

In Equation (22), E_i^t, $i = 1 \ldots 6$, are the six electric field amplitudes propagating in the symmetry directions (Figure 4). Combining Equations (3), (22) and (1), and assuming slowly varying amplitudes, the coupled-wave equations for TM modes in triangular lattice PC are obtained:

$$\begin{aligned} &-\frac{\partial}{\partial x}E_1^t + (\alpha - \alpha_L - \kappa_0 - i\delta)E_1^t \\ &= i\kappa_1\left(E_2^t + E_6^t\right) + i\kappa_2\left(E_3^t + E_5^t\right) + (i\kappa_3 - \kappa_0)\,E_4^t \qquad (23) \\ &-\frac{1}{2}\frac{\partial}{\partial x}E_2^t - \frac{\sqrt{3}}{2}\frac{\partial}{\partial y}E_2^t + (\alpha - \alpha_L - \kappa_0 - i\delta)\,E_2^t \\ &= i\kappa_1\left(E_1^t + E_3^t\right) + i\kappa_2\left(E_4^t + E_6^t\right) + (i\kappa_3 - \kappa_0)\,E_5^t \qquad (24) \\ &\frac{1}{2}\frac{\partial}{\partial x}E_3^t - \frac{\sqrt{3}}{2}\frac{\partial}{\partial y}E_3^t + (\alpha - \alpha_L - \kappa_0 - i\delta)\,E_3^t \\ &= i\kappa_1\left(E_2^t + E_4^t\right) + i\kappa_2\left(E_1^t + E_5^t\right) + (i\kappa_3 - \kappa_0)\,E_6^t \qquad (25) \\ &\frac{\partial}{\partial x}E_4^t + (\alpha - \alpha_L - \kappa_0 - i\delta)E_4^t \\ &= i\kappa_1\left(E_3^t + E_5^t\right) + i\kappa_2\left(E_2^t + E_6^t\right) + (i\kappa_3 - \kappa_0)\,E_1^t \qquad (26) \\ &\frac{1}{2}\frac{\partial}{\partial x}E_5^t + \frac{\sqrt{3}}{2}\frac{\partial}{\partial y}E_5^t + (\alpha - \alpha_L - \kappa_0 - i\delta)\,E_5^t \\ &= i\kappa_1\left(E_4^t + E_6^t\right) + i\kappa_2\left(E_1^t + E_3^t\right) + (i\kappa_3 - \kappa_0)\,E_2^t \qquad (27) \\ &-\frac{1}{2}\frac{\partial}{\partial x}E_6^t + \frac{\sqrt{3}}{2}\frac{\partial}{\partial y}E_6^t + (\alpha - \alpha_L - \kappa_0 - i\delta)\,E_6^t \\ &= i\kappa_1\left(E_1^t + E_5^t\right) + i\kappa_2\left(E_2^t + E_4^t\right) + (i\kappa_3 - \kappa_0)\,E_3^t \qquad (28) \end{aligned}$$

In Equations (23)–(28), as in the case of square lattice, δ is the Bragg frequency deviation, given by (17), while κ_1, κ_2, and κ_3 are the coupling coefficients, defined by (6), and expressed in, e.g., [19]. These coefficients describe strength and direction of the coupling of the waves, e.g., the coupling of E_1^t and E_4^t is described by κ_3, coupling of E_1^t, E_2^t, and E_6^t by κ_1, and coupling of E_1^t, E_3^t, and E_5^t by κ_2. In Equations (23)–(28), there is an additional coefficient κ_0 which, as in the square lattice case, is responsible for surface emission losses [7, 22].

Solution of Equations (23)–(28) for the boundary conditions

$$\begin{aligned} &E_1^t\left(-\frac{L}{2},y\right)=0, \quad E_2^t\left(-\frac{L}{2},y\right)=E_2^t\left(x,-\frac{L}{2}\right)=0,\\ &E_3^t\left(\frac{L}{2},y\right)=E_3^t\left(x,-\frac{L}{2}\right)=0, \quad E_4^t\left(\frac{L}{2},y\right)=0,\\ &E_5^t\left(\frac{L}{2},y\right)=E_5^t\left(x,\frac{L}{2}\right)=0, \quad E_6^t\left(-\frac{L}{2},y\right)=E_6^t\left(x,\frac{L}{2}\right)=0 \end{aligned} \tag{29}$$

defines structure eigenmodes at lasing threshold.

2.2.2. TE Polarization

In the triangular lattice photonic crystal cavity with TE polarization, the coupling process involves waves satisfying the same condition as it was stated in TM polarization case, i.e., ($|\mathbf{G}| = \beta_0$) [18],

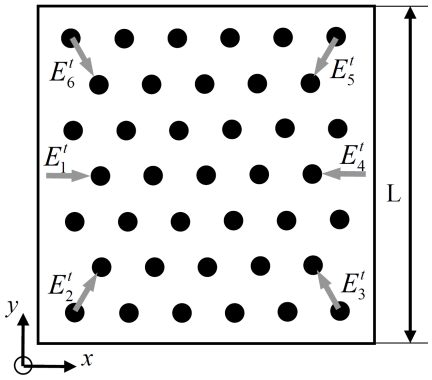

Figure 4. A schematic cross section of a triangular lattice photonic crystal laser active region, where the six basic waves involved in the coupling for TM polarization are shown.

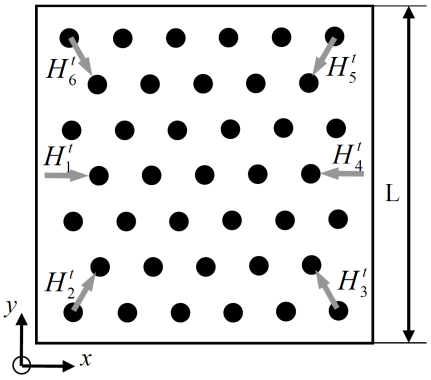

Figure 5. A schematic cross section of a triangular lattice photonic crystal laser active region, where the six basic waves involved in the coupling for TE polarization are shown.

neglecting higher order Bloch modes. Six basic waves most significantly contributing to coupling are depicted in Figure 5.

The magnetic field amplitudes $h(\mathbf{G})$ (Equation (8)) in the triangular lattice photonic crystal cavity are written as follows [18]:

$$H_z = H_1^t(x,y)e^{-i\beta_0 x} + H_2^t(x,y)e^{-i\frac{\beta_0}{2}x - i\frac{\sqrt{3}\beta_0}{2}y} + H_3^t(x,y)e^{i\frac{\beta_0}{2}x - i\frac{\sqrt{3}\beta_0}{2}y} + H_4^t(x,y)e^{i\beta_0 x} + H_5^t(x,y)e^{i\frac{\beta_0}{2}x + i\frac{\sqrt{3}\beta_0}{2}y} + H_6^t(x,y)e^{-i\frac{\beta_0}{2}x + i\frac{\sqrt{3}\beta_0}{2}y} \quad (30)$$

In Equation (43), H_i^t, $i = 1 \ldots 6$, are the six magnetic field amplitudes propagating in the symmetry directions (Figure 5). Combining Equations (4), (30) and (2), and assuming slowly varying magnetic field amplitudes, the coupled-wave equations for TE modes in triangular lattice PC are obtained:

$$\begin{aligned}
&-\frac{\partial}{\partial x}H_1^t + (\alpha - \alpha_L - \kappa_0 - i\delta)H_1^t \\
&= -i\frac{\kappa_1}{2}\left(H_2^t + H_6^t\right) + i\frac{\kappa_2}{2}\left(H_3^t + H_5^t\right) + (i\kappa_3 - \kappa_0)\,H_4^t \qquad (31)\\
&-\frac{1}{2}\frac{\partial}{\partial x}H_2^t - \frac{\sqrt{3}}{2}\frac{\partial}{\partial y}H_2^t + (\alpha - \alpha_L - \kappa_0 - i\delta)\,H_2^t \\
&= -i\frac{\kappa_1}{2}\left(H_1^t + H_3^t\right) + i\frac{\kappa_2}{2}\left(H_4^t + H_6^t\right) + (i\kappa_3 - \kappa_0)\,H_5^t \qquad (32)\\
&\frac{1}{2}\frac{\partial}{\partial x}H_3^t - \frac{\sqrt{3}}{2}\frac{\partial}{\partial y}H_3^t + (\alpha - \alpha_L - \kappa_0 - i\delta)\,H_3^t \\
&= -i\frac{\kappa_1}{2}\left(H_2^t + H_4^t\right) + i\frac{\kappa_2}{2}\left(H_1^t + H_5^t\right) + (i\kappa_3 - \kappa_0)\,H_6^t \qquad (33)\\
&\frac{\partial}{\partial x}H_4^t + (\alpha - \alpha_L - \kappa_0 - i\delta)H_4^t \\
&= -i\frac{\kappa_1}{2}\left(H_3^t + H_5^t\right) + i\frac{\kappa_2}{2}\left(H_2^t + H_6^t\right) + (i\kappa_3 - \kappa_0)\,H_1^t \qquad (34)\\
&\frac{1}{2}\frac{\partial}{\partial x}H_5^t + \frac{\sqrt{3}}{2}\frac{\partial}{\partial y}H_5^t + (\alpha - \alpha_L - \kappa_0 - i\delta)\,H_5^t \\
&= -i\frac{\kappa_1}{2}\left(H_4^t + H_6^t\right) + i\frac{\kappa_2}{2}\left(H_1^t + H_3^t\right) + (i\kappa_3 - \kappa_0)\,H_2^t \qquad (35)\\
&-\frac{1}{2}\frac{\partial}{\partial x}H_6^t + \frac{\sqrt{3}}{2}\frac{\partial}{\partial y}H_6^t + (\alpha - \alpha_L - \kappa_0 - i\delta)\,H_6^t \\
&= -i\frac{\kappa_1}{2}\left(H_1^t + H_5^t\right) + i\frac{\kappa_2}{2}\left(H_2^t + H_4^t\right) + (i\kappa_3 - \kappa_0)\,H_3^t \qquad (36)
\end{aligned}$$

where the coupling coefficients κ_1, κ_2, and κ_3 have the same physical meaning as described in the TM polarization case. The boundary conditions for the square region of PC with triangular symmetry are

written as:

$$\begin{aligned} &H_1^t\left(-\frac{L}{2},y\right)=0, \quad H_2^t\left(-\frac{L}{2},y\right)=H_2^t\left(x,-\frac{L}{2}\right)=0, \\ &H_3^t\left(\frac{L}{2},y\right)=H_3^t\left(x,-\frac{L}{2}\right)=0, \quad H_4^t\left(\frac{L}{2},y\right)=0, \\ &H_5^t\left(\frac{L}{2},y\right)=H_5^t\left(x,\frac{L}{2}\right)=0, \quad H_6^t\left(-\frac{L}{2},y\right)=H_6^t\left(x,\frac{L}{2}\right)=0. \end{aligned} \tag{37}$$

3. NUMERICAL ANALYSIS OF THE PC LASER THRESHOLD OPERATION

3.1. Square Lattice

3.1.1. TM Polarization

In Figure 6, an enlarged area of a square lattice photonic crystal dispersion curves for the first four modes (A, B, C, D) in the vicinity of Γ point is shown. The plane wave method [23] was used to plot the dispersion characteristic for the infinite two-dimensional PC structure with circular holes $\varepsilon_b = 9.8$ arranged in square lattice with background material $\varepsilon_a = 12.0$. The ratio of rods radius to lattice constant was set to 0.24, and the number of plane waves was set at about 1024.

In Figure 6, each of the selected (A, B, C, D) points represents a mode, characterized by Bragg frequency deviation δ, threshold gain

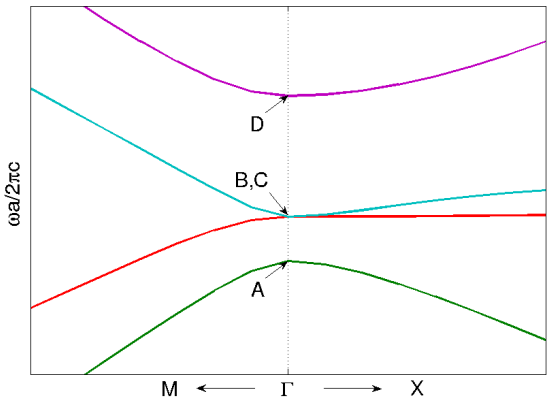

Figure 6. An enlarged area of a square lattice photonic crystal dispersion curves for the first four modes in the vicinity of Γ point. Square lattice, TM polarization.

α, and threshold field distribution. These characteristic values were calculated by the numerical solution of Equations (10)–(13). In order to assign appropriate points A, B, C, D to the obtained numerical values, it was necessary to use the analytic expressions for the Bragg frequency deviation [15]:

$$\delta_{\mathrm{A}} = -2\kappa_2 - \kappa_3, \quad \delta_{\mathrm{B,C}} = \kappa_3, \quad \delta_{\mathrm{D}} = 2\kappa_2 - \kappa_3. \tag{38}$$

These expressions were obtained from Equations (10)–(13) where no gain ($\alpha = 0$), no loss ($\kappa_0 = 0$, $\alpha_L = 0$), and no spatial dependence of electric field amplitude were assumed.

Equations (10)–(13) were solved numerically for the wide range of coupling coefficients (κ_2, κ_3), obtaining solutions $((\delta, \alpha, E_l^s)^j)_{\kappa_{3i}}$, where $l = 1, 2, 3, 4$, κ_{3i} corresponds to subsequent values of coupling coefficient for different modes j = A, B, C, D. Assigning numerical values of δ_j to analytical solutions (38), the mode structure of 2D square lattice PC laser with TM polarization has been obtained.

Figure 7 shows the field distributions $|E_1^s|^2 + |E_2^s|^2 + |E_3^s|^2 + |E_4^s|^2$ corresponding to modes: A — Figure 7(a), D — Figure 7(b), B, C — Figures 7(b), (c). They were made for the normalized coupling coefficients $|\kappa_2 L| = 8$, $|\kappa_3 L| = 4$ and filling factor $f = 0.16$.

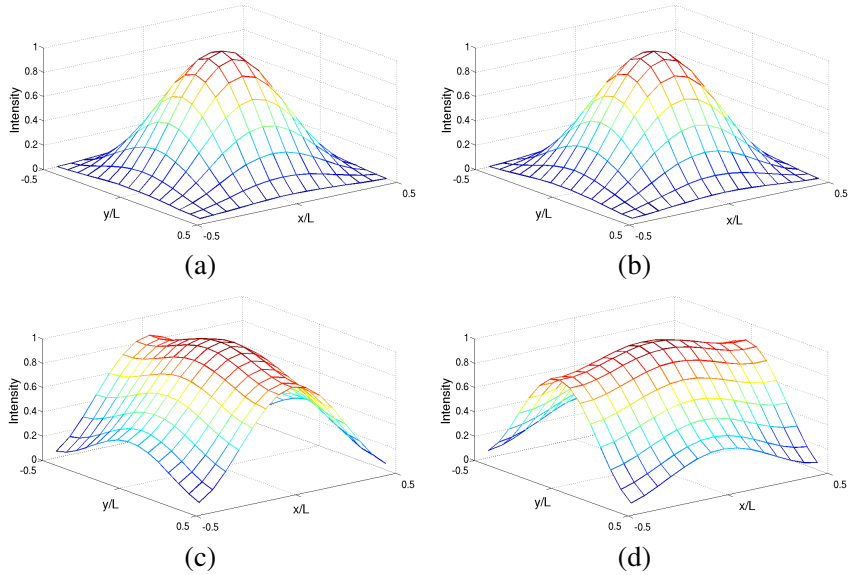

Figure 7. Electromagnetic field distributions corresponding to (a) A, (b) D, (c) B, and (d) C points from Figure 6, respectively.

In Figure 8, the normalized threshold gain α_L was plotted as a function of Bragg frequency deviation δ, for various values of the normalized coupling coefficient $\kappa_3 L$ (which takes values from 0.01 to 50).

Figure 8 shows that increasing values of coupling coefficient refer to the Bragg frequency deviation increment and threshold gain decrement. Simultaneously for larger values of coupling coefficient, the threshold gain tends to be similar values. It is also worth noting that the threshold gain values for mode A are the lowest in vide range of coupling coefficient.

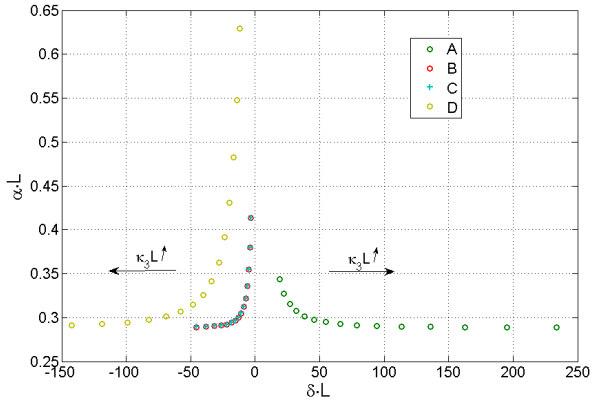

Figure 8. The dependence of threshold gain versus Bragg frequency deviation.

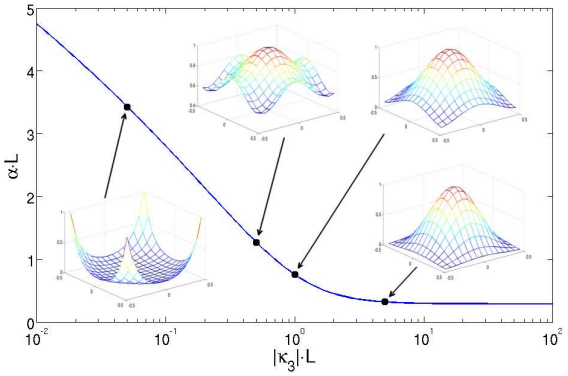

Figure 9. Mode A development for increasing values of coupling coefficient.

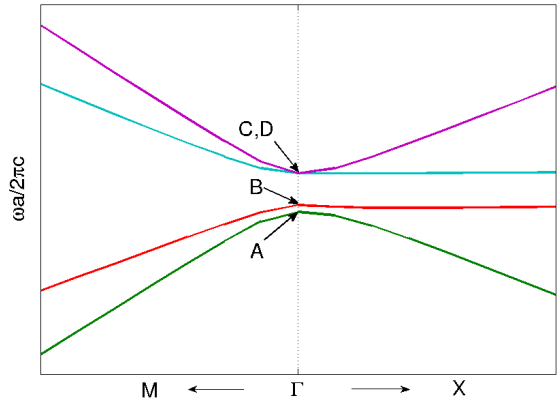

Figure 10. An enlarged area of a square lattice photonic crystal dispersion curves for the first four modes in the vicinity of Γ point. Square lattice, TE polarization.

Figure 9 illustrates mode A (shown in Figure 6) development on the threshold gain α vs. coupling coefficient κ_3 curve.

3.1.2. TE Polarization

In Figure 10, similar as in TM polarization case, an enlarged area of a square lattice photonic crystal dispersion curves for the first four modes (A, B, C, D) in the vicinity of Γ point is shown. The plane wave method [23] was used with the same parameters as done for TM polarization.

Each of the selected (A, B, C, D) points represents a mode, characterized by Bragg frequency deviation δ, threshold gain α, and threshold field distribution. These characteristic values were calculated by the numerical solution of Equations (17)–(20). In order to assign appropriate points A, B, C, D to the obtained numerical values, as for TM polarization, it was necessary to use the analytic expressions for the Bragg frequency deviation [17]:

$$\delta_{\mathrm{A}} = -\frac{8\kappa_1^2}{\beta_0} - \kappa_3, \quad \delta_{\mathrm{B}} = -\kappa_3, \quad \delta_{\mathrm{C,D}} = -\frac{4\kappa_1^2}{\beta_0} + \kappa_3. \tag{39}$$

These expressions were obtained from Equations (17)–(20) where no gain ($\alpha = 0$), no loss ($\kappa_0 = 0$, $\alpha_L = 0$), and no spatial dependence of magnetic field amplitude were assumed.

Equations (17)–(20) were solved numerically for the wide range of coupling coefficients (κ_1, κ_3), obtaining solutions $((\delta, \alpha, H_l^s)^j)_{\kappa_{3i}}$, where $l = 1, 3, 5, 7$, κ_{3i} corresponds to subsequent values of coupling coefficient for different modes j = A, B, C, D. Assigning numerical values of δ_j to analytical solutions (39), the mode structure of 2D square lattice PC laser with TE polarization has been obtained. Figure 11 shows the field distributions $|H_1^s|^2 + |H_3^s|^2 + |H_5^s|^2 + |H_7^s|^2$ corresponding to modes: A — Figure 11(a), B — Figure 11(b), C, D — Figures 11(c), (d). They were made for the normalized coupling coefficients $|\kappa_1 L| = 10.96$, $|\kappa_3 L| = 4$ and filling factor $f = 0.16$.

In Figure 12, the normalized threshold gain α_L was plotted as a function of Bragg frequency deviation δ, for various values of the normalized coupling coefficient $\kappa_3 L$ (which takes values from 0.01 to 50).

Figure 12 shows that increasing values of coupling coefficient refer to the Bragg frequency deviation increment and the threshold gain decrement. Simultaneously, for larger values of coupling coefficient the threshold gain tends to be similar values.

Figure 13 depicts mode A (shown in Figure 10) development with increasing values of coupling coefficient κ_3 on the threshold gain α curve. Compared to square lattice transverse magnetic polarization

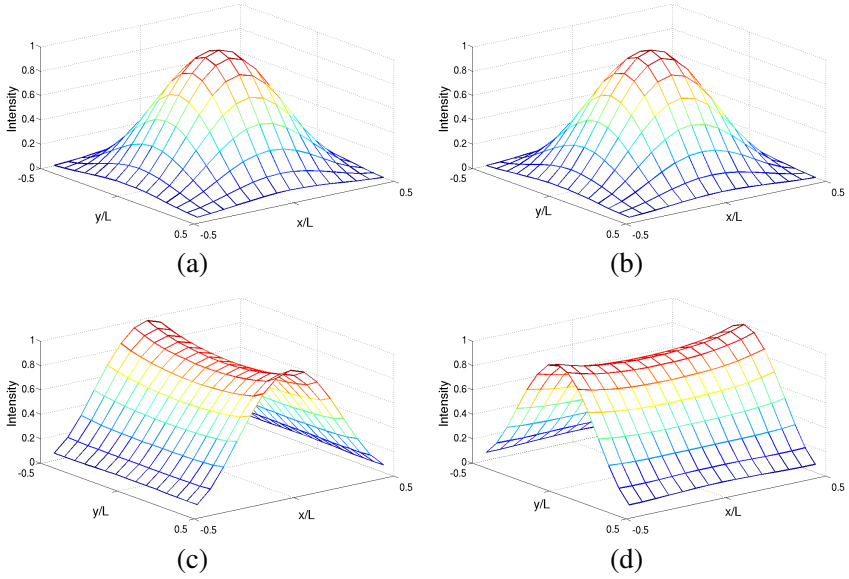

Figure 11. Electromagnetic field distributions corresponding to (a) A, (b) B, (c) C, and (d) D points from Figure 10, respectively.

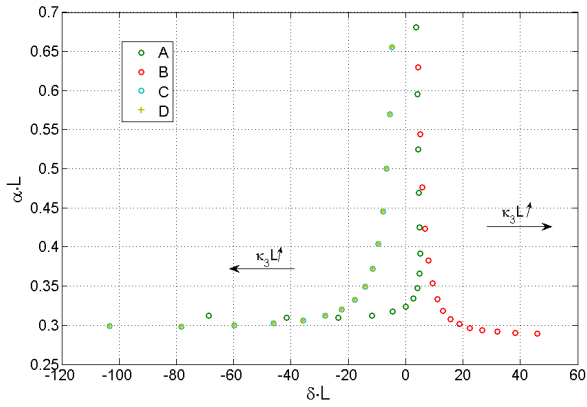

Figure 12. The dependence of threshold gain versus Bragg frequency deviation.

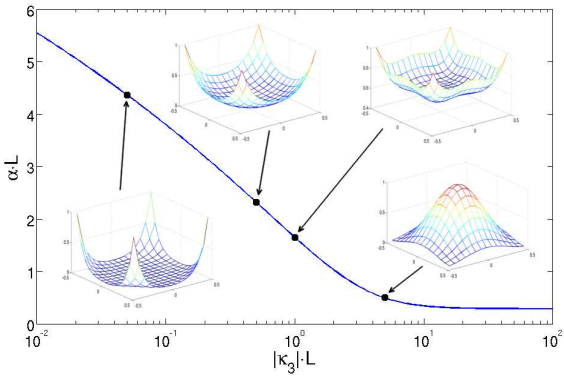

Figure 13. Mode A development for increasing values of coupling coefficient.

case, it is noticed that TE modes develop higher field confinement in the structure for the greater difference of refractive indices (i.e., higher values of coupling coefficient).

3.2. Triangular Lattice

3.2.1. TM Polarization

Similar as in case of square lattice, in Figure 14 an enlarged area of a triangular lattice photonic crystal dispersion curves for the first six

modes (A, B, C, D, E, F) in the vicinity of Γ point is shown. The plane wave method [23] was used to plot the dispersion characteristic for the infinite two-dimensional PC structure with circular holes $\varepsilon_b = 9.8$ arranged in triangular lattice with background material $\varepsilon_a = 12.0$. The ratio of rods radius to lattice constant was set to 0.24, and the number of plane waves to 1024.

In Figure 14, each of the selected (A, B, C, D, E, F) points represents a mode, characterized by Bragg frequency deviation δ, threshold gain α, and threshold field distribution. These characteristic values were calculated by the numerical solution of Equations (23)–(28). In order to assign appropriate points A, B, C, D, E, F to the obtained numerical values, it was necessary to express the Bragg frequency deviation through the coupling coefficients:

$$\begin{aligned} \delta_{\mathrm{A}} &= -2\kappa_1 - 2\kappa_2 - \kappa_3, \quad \delta_{\mathrm{B,C}} = -\kappa_1 + \kappa_2 + \kappa_3, \\ \delta_{\mathrm{D,E}} &= \kappa_1 + \kappa_2 - \kappa_3, \quad \delta_{\mathrm{F}} = 2\kappa_1 - 2\kappa_2 + \kappa_3. \end{aligned} \tag{40}$$

Similar to previous cases, expressions (40) were obtained from coupled-mode Equations (23)–(28) where no gain ($\alpha = 0$), no loss ($\kappa_0 = 0$, $\alpha_L = 0$), and no spatial dependence of electric field amplitude were assumed. Equations (23)–(28) were solved numerically for the wide range of coupling coefficients (κ_1, κ_2, κ_3), obtaining solutions $((\delta, \alpha, E_k^t)^j)_{\kappa_{3i}}$, where κ_{3i} corresponds to subsequent values of coupling coefficient for different modes j = A, B, C, D, E, F; $k = 1 \ldots 6$. Assigning numerical values of δ_j to the analytical solutions (40), the

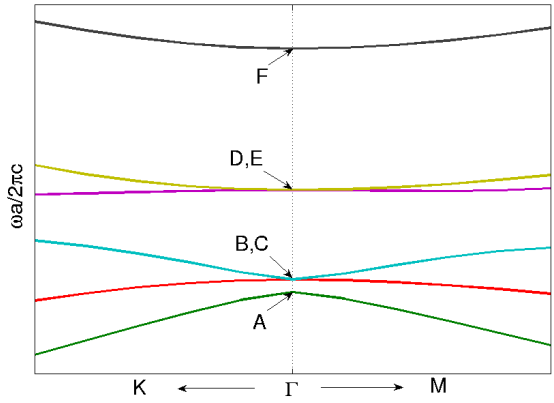

Figure 14. An enlarged area of dispersion curves of photonic crystal for the first six modes in the vicinity of Γ point. Triangular lattice, TM polarization.

mode structure of 2D triangular lattice PC laser with TM polarization has been obtained. Figure 15 shows the field distributions $\sum_{i=1}^{6} |E_i^t|^2$ corresponding to the modes: A — Figure 15(a), F — Figure 15(b), B, C — Figures 15(c), (d), D, E — Figures 15(e), (f). They were made for the normalized coupling coefficients $|\kappa_1 L| = 13.96$, $|\kappa_2 L| = 6.6$, $|\kappa_3 L| = 4$, and filling factor $f = 0.16$.

In Figure 16, the normalized threshold gain α_L was plotted as a function of Bragg frequency deviation δ, for various values of the normalized coupling coefficient $\kappa_3 L$ (which takes values from 0.01 to 50).

Figure 16 shows that increasing values of coupling coefficient refer

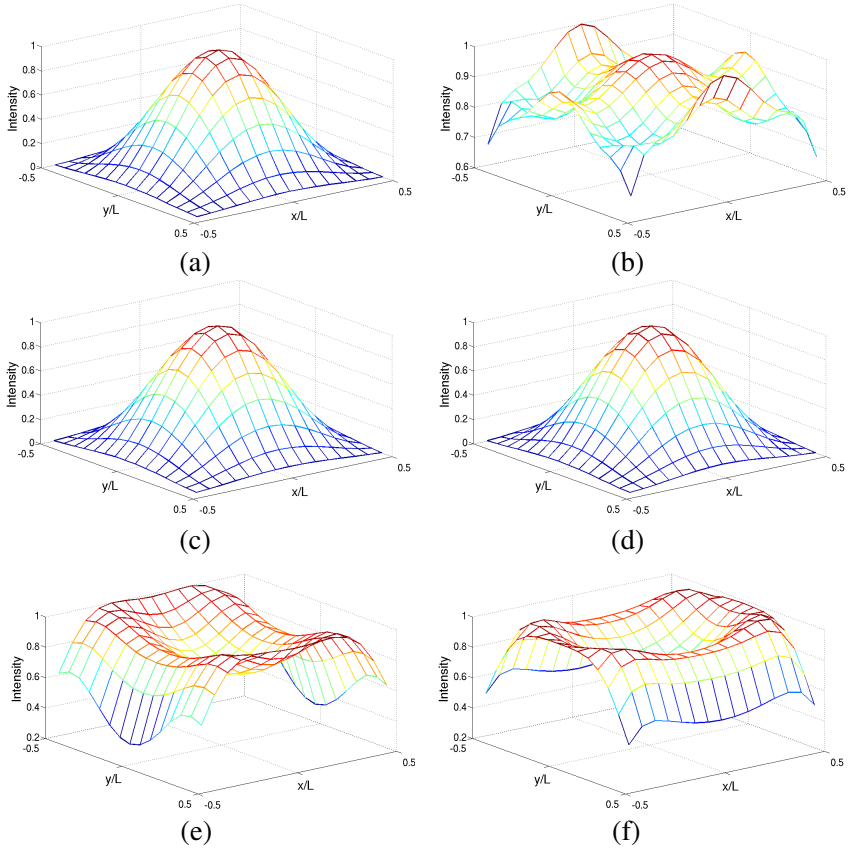

Figure 15. Electromagnetic field distributions corresponding to (a) A, (b) F, (c) B, (d) C, (e) D, and (f) E points from Figure 14, respectively.

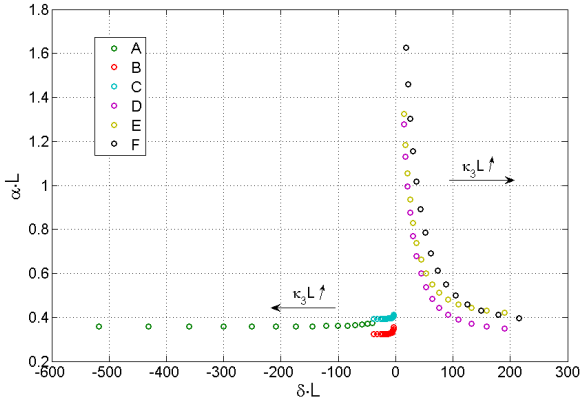

Figure 16. The dependence of threshold gain versus Bragg frequency deviation.

to the Bragg frequency deviation increment and the threshold gain decrement. Simultaneously, for larger values of coupling coefficient the threshold gain tends to be similar values. The difference in the values of degenerate modes' threshold gains stem from numerical inaccuracy.

Similar as shown in square lattice case, here in Figure 17 mode A (showed in Figure 14) development is shown on the threshold gain α vs. coupling coefficient κ_3 curve.

3.2.2. TE Polarization

In Figure 18, an enlarged area of a triangular lattice photonic crystal dispersion curves for the first six modes (A, B, C, D, E, F) in the vicinity of Γ point is shown. The plane wave method was used to plot the dispersion characteristic with the same parameters as done for TM polarization.

In Figure 18, each of the selected points (A, B, C, D, E, F) represents a mode, characterized by Bragg frequency deviation δ, threshold gain α, and threshold field distribution. These characteristic values were calculated by the numerical solution of Equations (31)–(36). In order to assign appropriate points A, B, C, D, E, F to the obtained numerical values, it was necessary to express Bragg frequency deviation through the coupling coefficients:

$$\begin{aligned} \delta_{\mathrm{A}} &= -\kappa_1 - \kappa_2 + \kappa_3, \quad & \delta_{\mathrm{B,C}} &= -\frac{\kappa_1}{2} + \frac{\kappa_2}{2} - \kappa_3, \\ \delta_{\mathrm{D}} &= \kappa_1 - \kappa_2 - \kappa_3, & \delta_{\mathrm{E,F}} &= \frac{\kappa_1}{2} + \frac{\kappa_2}{2} + \kappa_3. \end{aligned} \tag{41}$$

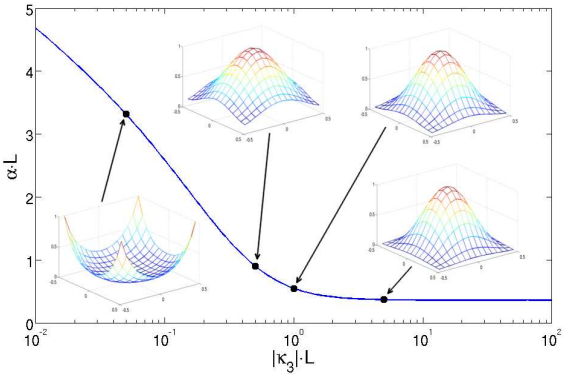

Figure 17. Mode A development for increasing values of coupling coefficient.

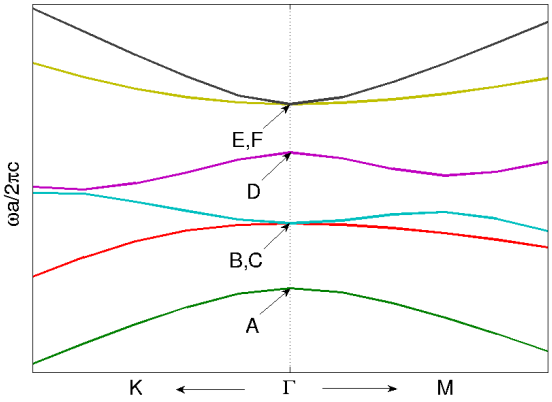

Figure 18. An enlarged area of dispersion curves of photonic crystal for the first six modes in the vicinity of Γ point. Triangular lattice, TE polarization.

Expressions (41) were obtained from coupled mode Equations (31)–(36) where no gain ($\alpha = 0$), no loss ($\kappa_0 = 0$, $\alpha_L = 0$), and no spatial dependence of magnetic field amplitude were assumed. Equations (31)–(36) were solved numerically for the wide range of coupling coefficients (κ_1, κ_2, κ_3), obtaining solutions $((\delta, \alpha, H_k^t)^j)_{\kappa_{3i}}$, where κ_{3i} corresponds to subsequent values of coupling coefficient for different modes j = A, B, C, D, E, F; $k = 1 \ldots 6$. Assigning numerical values of

δ_j to the analytical solutions (41), the mode structure of 2D triangular lattice PC laser with TE polarization has been obtained. Figure 19 shows the field distributions $\sum_{i=1}^{6} |H_i^t|^2$ corresponding to the modes: A — Figure 19(a), D — Figure 19(b), B, C — Figures 19(c), (d), E, F — Figures 19(e), (f).

Plots in Figure 19 were made for the same normalized coupling coefficients as in the case of TM polarization, i.e., $|\kappa_1 L| = 13.96$, $|\kappa_2 L| = 6.6$, $|\kappa_3 L| = 4$, and filling factor $f = 0.16$.

In Figure 20, the normalized threshold gain α_L was plotted as a function of Bragg frequency deviation δ, for various values of the

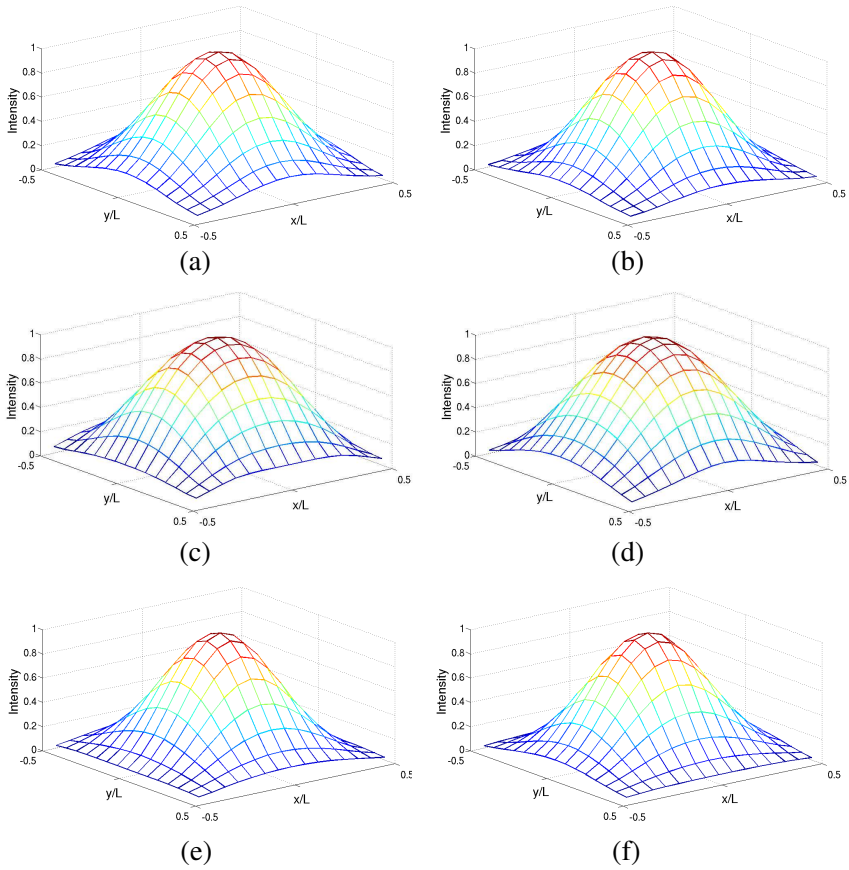

Figure 19. Electromagnetic field distributions corresponding to (a) A, (b) D, (c) B, (d) C, (e) E, and (f) F points from Figure 18, respectively.

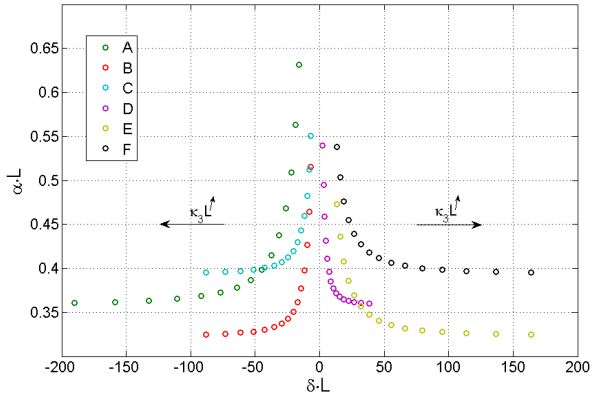

Figure 20. The dependence of threshold gain versus Bragg frequency deviation.

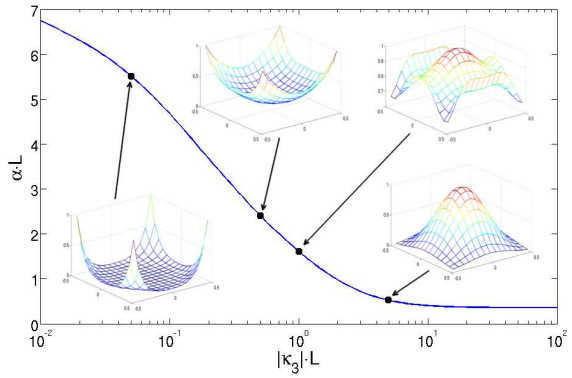

Figure 21. Mode A development for increasing values of coupling coefficient.

normalized coupling coefficient $\kappa_3 L$ (which takes values from 0.01 to 50).

Figure 20 shows that increasing values of coupling coefficient refer to the Bragg frequency deviation increment and threshold gain decrement. Simultaneously, for larger values of coupling coefficient the threshold gain tends to be similar values. The difference in the values of degenerate modes' threshold gains stem from numerical inaccuracy.

Figure 21 illustrates mode A (showed in Figure 18) development with increasing values of coupling coefficient κ_3 on the threshold gain

α curve. Compared to TM polarization case, as in square symmetry structures, it can be noticed that TE modes develop higher field confinement in the structure for the greater difference of refractive indices (i.e., higher values of coupling coefficient). Thus in general it can be stated that TM modes are better confined in the structures with small refractive indices difference.

4. CONCLUSIONS

We have presented a coupled-wave analysis for square and triangular lattices photonic crystal laser with TE and TM polarization. We used coupled-mode equations to analyze PC structures in the wide range of coupling coefficient values distinguishing basic modes. We have plotted threshold characteristics showing lowest threshold modes and their frequency deviations. We also illustrate the lowest frequency mode development with increasing values of coupling coefficient and point out that TM modes are most likely to occur in structures with low dielectric constants contrast.

REFERENCES

1. Miyai, E., K. Sakai, T. Okano, W. Kunishi, D. Ohnishi, and S. Noda, "Lasers producing tailored beams," *Nature*, Vol. 441, 946, 2006.
2. Sakai, K., E. Miyai, T. Sakaguchi, D. Ohnishi, T. Okano, and S. Noda, "Lasing band-edge identification for a surface-emitting photonic crystal laser," *IEEE J. Sel. Areas Commun.*, Vol. 23, No. 7, 1335–1340, 2005.
3. Imada, M., S. Noda, A. Chutinan, T. Tokuda, M. Murata, and G. Sasaki, "Coherent two-dimensional lasing action in surface-emitting laser with triangular-lattice photonic crystal structure," *Appl. Phys. Lett.*, Vol. 75, No. 3, 316–318, 1999.
4. Meier, M., A. Mekis, A. Dodabalapur, A. Timko, R. E. Slusher, J. D. Joannopoulos, and O. Nalamasu, "Laser action from two-dimensional distributed feedback in photonic crystals," *Appl. Phys. Lett.*, Vol. 74, No. 1, 7–9, 1999.
5. Noda, S., M. Yokoyama, M. Imada, A. Chutinan, and M. Mochizuki, "Polarization mode control of two-dimensional photonic crystal laser by unit cell structure design," *Science*, Vol. 293, No. 5532, 1123–1125, 2001.
6. Turnbull, G. A., P. Andrew, W. L. Barnes, and I. D. W. Samuel, "Operating characteristics of a semiconducting polymer laser

pumped by a microchip laser," *Appl. Phys. Lett.*, Vol. 82, No. 3, 313–315, 2003.

7. Vurgaftman, I. and J. R. Meyer, "Design optimization for high-brightness surface-emitting photonic-crystal distributed-feedback lasers," *IEEE J. Quantum Electron.*, Vol. 39, No. 6, 689–700, 2003.
8. Ohnishi, D., T. Okano, M. Imada, and S. Noda, "Room temperature continuous wave operation of a surface-emitting two-dimensional photonic crystal diode laser," *Opt. Express*, Vol. 12, No. 8, 1562–1568, 2004.
9. Matsubara, H., S. Yoshimoto, H. Saito, Y. Jianglin, Y. Tanaka, and S. Noda, "GaN photonic-crystal surface-emitting laser at blue-violet wavelengths," *Science*, Vol. 319, No. 5862, 445–447, 2008.
10. Lu, T. C., S. W. Chen, L. F. Lin, T. T. Kao, C. C. Kao, P. Yu, H. C. Kuo, and S. C. Wang, "GaN-based two-dimensional surface-emitting photonic crystal lasers with AlN/GaN distributed Bragg reflector," *Appl. Phys. Lett.*, Vol. 92, No. 1, 011129 1–3, 2008.
11. Kim, M., C. S. Kim, W. W. Bewley, J. R. Lindle, C. L. Canedy, I. Vurgaftman, and J. R. Meyer, "Surface emitting photonic-crystal distributed-feedback laser for the midinfrared," *Appl. Phys. Lett.*, Vol. 88, No. 19, 191105 1–3, 2006.
12. Imada, M., A. Chutinan, S. Noda, and M. Mochizuki, "Multidirectionally distributed feedback photonic crystal lasers," *Phys. Rev. B*, Vol. 65, No. 19, 195306 1–8, 2002.
13. Yokoyama, M. and S. Noda, "Finite-difference time-domain simulation of two-dimensional photonic crystal surface-emitting laser," *Opt. Express*, Vol. 13, No. 8, 2869–2880, 2005.
14. Plihal, M. and A. A. Maradudin, "Photonic band structure of two-dimensional systems: The triangular lattice," *Phys. Rev. B*, Vol. 44, No. 16, 8565–8571, 1991.
15. Sakai, K., E. Miyai, and S. Noda, "Coupled-wave model for square-lattice two-dimensional photonic crystal with transverse-electric-like mode," *Appl. Phys. Lett.*, Vol. 89, No. 2, 021101 1–3, 2006.
16. Sakai, K., E. Miyai, and S. Noda, "Coupled-wave theory for square-lattice photonic crystal lasers with TE polarization," *IEEE J. Quantum Electron.*, Vol. 46, No. 5, 788–795, 2010.
17. Sakai, K., E. Miyai, and S. Noda, "Two-dimensional coupled wave theory for square-lattice photonic-crystal lasers with TM-polarization," *Opt. Express*, Vol. 15, 3981–3990, 2007.

18. Sakai, K., J. Yue, and S. Noda, "Coupled-wave model for triangular-lattice photonic crystal with transverse electric polarization," *Opt. Express*, Vol. 16, No. 9, 6033–6040, 2008.
19. Koba, M., P. Szczepanski, and T. Kossek, "Nonlinear operation of a 2D triangular lattice photonic crystal laser," *IEEE J. Quantum Electron.*, Vol. 47, No. 1, 13–19, 2011.
20. Scamarcio, G., F. Capasso, C. Sirtori, J. Faist, A. L. Hutchinson, D. L. Sivco, and A. Y. Cho, "High-power infrared (8-micrometer wavelength) superlattice lasers," *Science*, Vol. 276, No. 5313, 773–776, 1997.
21. Kogelnik, H., "Coupled wave theory for thick hologram gratings," *Bell Syst. Tech. J.*, Vol. 48, 2909–2947, 1969.
22. Kazarinov, R. and C. Henry, "Second-order distributed feedback lasers with mode selection provided by first-order radiation losses," *IEEE J. Quantum Electron.*, Vol. 21, No. 2, 144–150, 1985.
23. Johnson, S. and J. Joannopoulos, "Block-iterative frequency-domain methods for Maxwell's equations in a planewave basis," *Opt. Express*, Vol. 8, No. 10, 173–190, 2001.
24. Liang, Y., C. Peng, K. Sakai, S. Iwahashi, and S. Noda, "Three-dimensional coupled-wave model for square-lattice photonic crystal lasers with transverse electric polarization: A general approach," *Phys. Rev. B*, Vol. 84, No. 19, 195119 1–11, 2011.
25. Peng, C., Y. Liang, K. Sakai, S. Iwahashi, and S. Noda, "Coupled-wave analysis for photonic-crystal surface-emitting lasers on air holes with arbitrary sidewalls," *Opt. Express*, Vol. 19, No. 24, 24672–24686, 2011.